24 Ma Giant Copper polymetallic porphyry-related breccia of the ancestral Cascades, southwest British Columbia

Mitchell G. Mihalynuk[1, a], and Janet E. Gabites[2, *]

[1] British Columbia Geological Survey, Ministry of Mining and Critical Minerals, Victoria, BC, V8W 9N3
[2] Pacific Centre for Isotopic and Geochemical Research, Department of Earth, Ocean and Atmospheric Sciences, The University of British Columbia, Vancouver, BC, V6T 1Z4
* retired
[a] corresponding author: Mitch.Mihalynuk@gov.bc.ca

Recommended citation: Mihalynuk, M.G., and Gabites, J.E., 2026. 24 Ma Giant Copper polymetallic porphyry-related breccia of the ancestral Cascades, southwest British Columbia. In: Geological Fieldwork 2025, British Columbia Ministry of Mining and Critical Minerals, British Columbia Geological Survey Paper 2026-01, pp. 163-174.

Abstract

A recent metallogenic study of mineralized breccias at Giant Copper in southwestern British Columbia suggested that the Invermay magmatic suite (24.9 ±0.2 Ma, late Oligocene) is responsible for mineralization. We corroborate this inference by $^{40}Ar/^{39}Ar$ (biotite) geochronology on both the Invermay magmatic suite and the mineralization. Ar release spectra from the intrusion and two from mineralized samples yield ages of 24.22 ±0.15 Ma, 24.87 ±0.33 Ma, and 24.08 ±0.19 Ma. Copper-silver-gold-bearing breccias of Giant Copper are the northernmost known (49.16°N) part of the ancestral Cascade belt of porphyry-related deposits defined in Washington state. However, Oligocene magmatic rocks, some with past-producing mineral deposits, span the length of western British Columbia.

Keywords: Giant Copper, porphyry copper, copper-silver-gold tourmaline breccia, $^{40}Ar/^{39}Ar$ geochronology, Oligocene, thermochronology, Invermay magmatic suite, ancestral Cascade porphyry belt, Hozameen terrane, Bridge River terrane, Methow basin, Ladner Group, Dewdney Creek Formation

1. Introduction

Giant Copper is a tourmaline-magnetite breccia-hosted deposit in southwest British Columbia, 37 km southeast of Hope and 20 km north of the US border (Figs. 1, 2) in an area that includes the lands and traditional territories of many Indigenous rights holders. The deposit has an indicated resource of 45.37 million tonnes grading 0.47% copper, 11.19 g/t silver, and 0.38 g/t gold (Pinsent, 1998). In addition, zinc (in sphalerite) is commonly found in the breccia pipes, and some zones contain molybdenite (±associated uraninite) and galena. At the time of our sampling (2006), the mineral tenures were surrounded by parkland (Skagit River Park to the west and Manning Park on all other sides). However, the claims have since been surrendered to the Province of British Columbia (Imperial Metals Corporation, 2022).

Mineralization at Giant Copper is concentrated in a cluster of seven breccia bodies (Fig. 3). The first was discovered in 1930, the AM breccia (MINFILE 092HSW001), followed by the Invermay breccia in 1933 (MINFILE 092HSW002). Mineral production has only been recorded from the Invermay body, which generated 94 metric tonnes of ore between 1936 and 1947, from which 10.6 tonnes of zinc, 9.65 tonnes of lead, 313 kg of silver and 0.7 kg of gold were recovered (copper production is not reported, MINFILE 092HSW002). Since 1947, mineral exploration at Giant Copper has been intermittent (Robertson, 2006), with the last major effort including drilling and production of a digital map, conducted in 1996 by Imperial Minerals Corp., followed by geochemical surveys in 2015 (Miller-Tait, 2016). Recent metallogenic study of the Giant Copper tourmaline breccia pipes (Fischer, 2022; Fischer et al., 2023, 2024) focused primarily on the AM body, which is analogous to other porphyry-related pipes globally, such as those at the world's third largest porphyry copper deposit, Rio Blanco-Los Bronces, in Chile (Frikken et al., 2005).

Laser ablation ICP-MS dating of the Invermay intrusive suite at Giant Copper by Fischer (2022) produced a weighted mean U-Pb age of 24.9 ±0.2 Ma (from 99 zircon grains). Such a young age was unexpected because previous work inferred a Cretaceous age (e.g., Robertson, 2006; Miller-Tait, 2016). Based on the assumption that the intrusive suite dated was the source of mineralization, this Oligocene date (time scale of Cohen et al., 2025) was taken to be the maximum limit on mineralized breccia pipe formation (Fischer, 2022). Herein we present $^{40}Ar/^{39}Ar$ (biotite) geochronologic data from three Invermay magmatic suite samples including two that provide estimates for the time of mineralization. Our results confirm the previous U-Pb dates for the intrusion (Fischer, 2022) and indicate that mineralization was penecontemporaneous with emplacement of the Invermay body.

2. Regional geologic setting

Following early transect and 4-mile mapping by Cairnes (1924, 1944), many workers have contributed to understanding

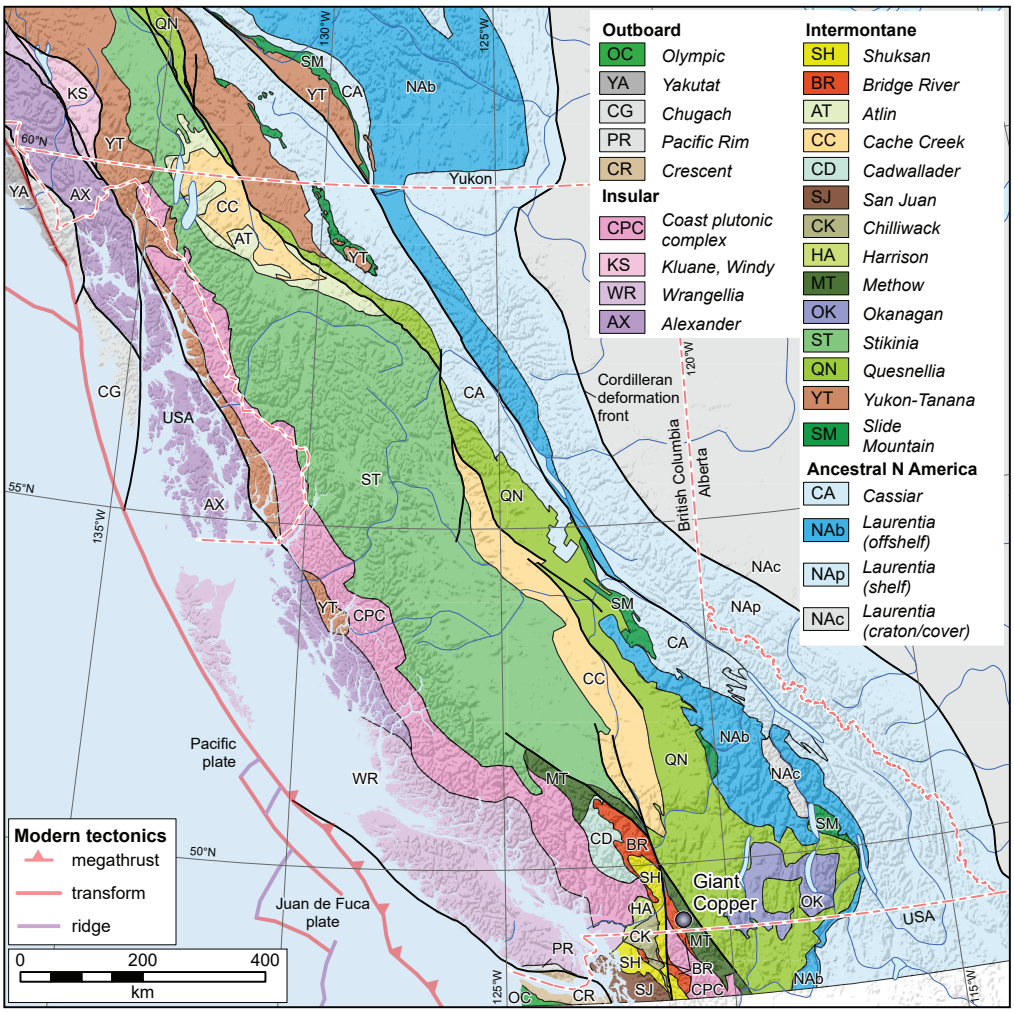

Fig. 1. Location of study area. Terranes (modified from Colpron, 2020; after Wheeler et al., 1991; Zagorevski et al., 2021).

the regional geology of Giant Copper including: 1:50,000-scale mapping of Manning Park by Coates (1974); 1:250,000-scale mapping of the Hope map sheet by Monger (1989); and 1:20,000-scale mapping of the Cascade Recreational area by Schmitt and Koyanagi (1992). Property-scale mapping (e.g., Miller-Tait 2016) added significant details.

Three main rock packages form basement across the area (Fig. 3). The oldest of these is in the west, the Hozameen Group (commonly spelled Hozomeen in US), which includes deep-marine sedimentary rocks and ophiolitic rocks having ocean island to island arc tholeiite chemistry (Ray, 1990). These rocks represent the Hozameen terrane which is interpreted as equivalent to the Bridge River terrane from which it has been offset by the Fraser-Straight Creek fault (Umhoefer and Miller, 1996; Umhoefer and Schiarizza, 1996; Fig. 3). Fossils in chert and sparse limestone beds are Pennsylvanian to Late Jurassic (Haugerud and Tabor, 2009).

Bounding Hozameen terrane on its east is the Hozameen fault, delineated by a belt of serpentinite bodies (Ray, 1986) and separating it from the Jura-Cretaceous strata of the Methow terrane. At the latitude of Figure 3, Methow basin is equivalent to the Methow terrane. The basin may have been floored by Triassic mid-ocean ridge basalts (Spider Peak Formation; Ray, 1990) and was filled in the Early Jurassic by lower Ladner Group turbiditic marine siliciclastic deposits, followed by volcaniclastic-rich strata of the Dewdney Creek Formation (Middle to Late Jurassic; cf. O'Brien, 1987; O'Brien et al., 1992). Wacke and coarse polymictic conglomerate of the Jackass Mountain Group (Early Cretaceous) overlie the Methow terrane and are interpreted to have been derived from proximal eastern sources that were isolated from the craton (Surpless et al., 2014).

The eastern limits of the Methow terrane are mostly defined by the Pasayten fault which separates the terrane from the highly attenuated composite plutons of the Eagle plutonic complex that young to the south (Late Jurassic to Early Cretaceous; Greig et al., 1992; Hurlow and Nelson, 1993). The Eagle complex was underthrust by the western edge of Quesnel terrane, which was subjected to medium-pressure amphibolite-grade metamorphism (Oliver, 2011).

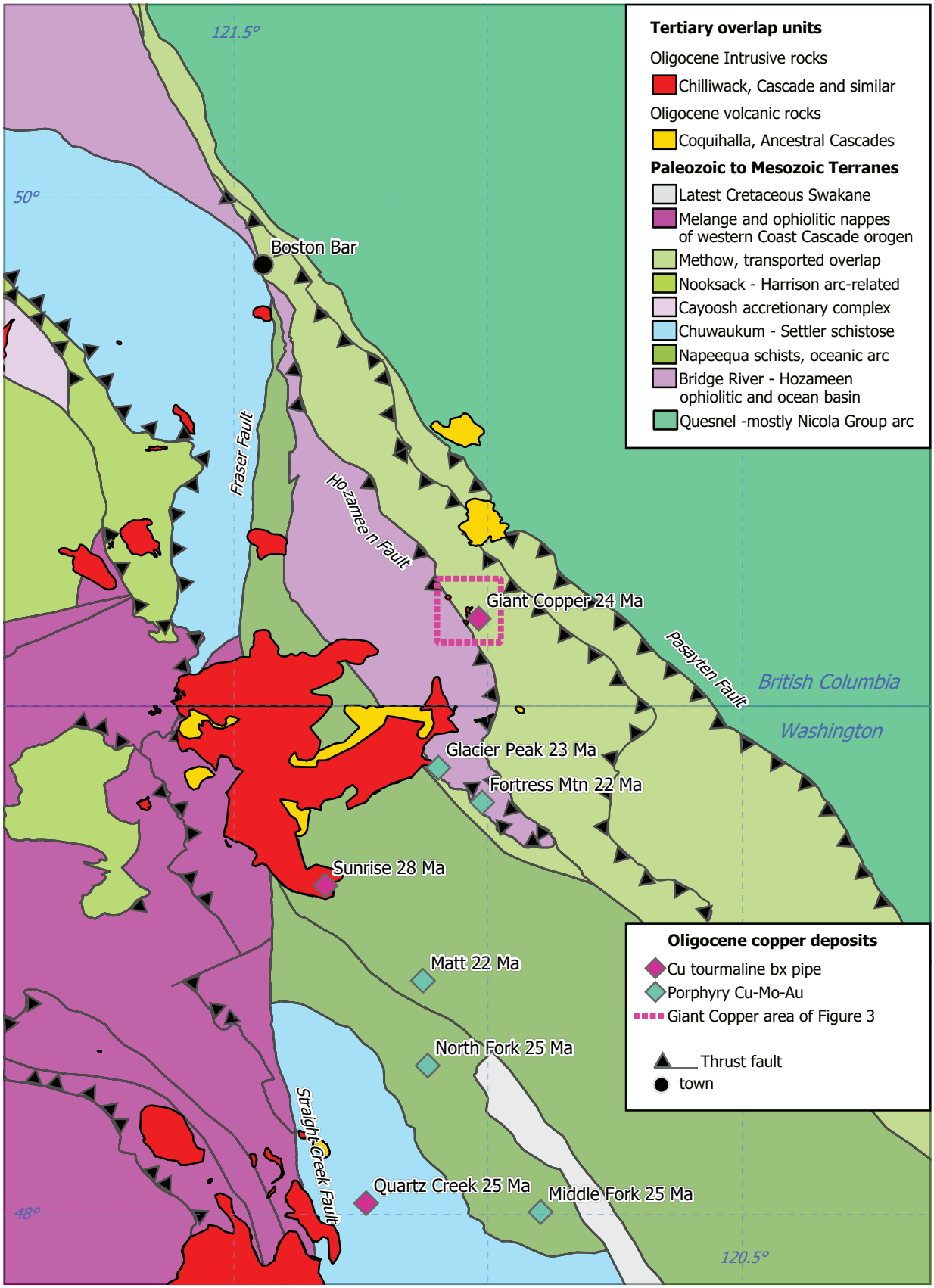

Fig. 2. Regional geological setting of the Giant Copper deposit based on work by Cairnes (1920, 1924, 1929, 1944), Tabor et al. (2003), Haugerud and Tabor (2009), Monger and Brown (2016), and Tabor and Haugerud (2016).

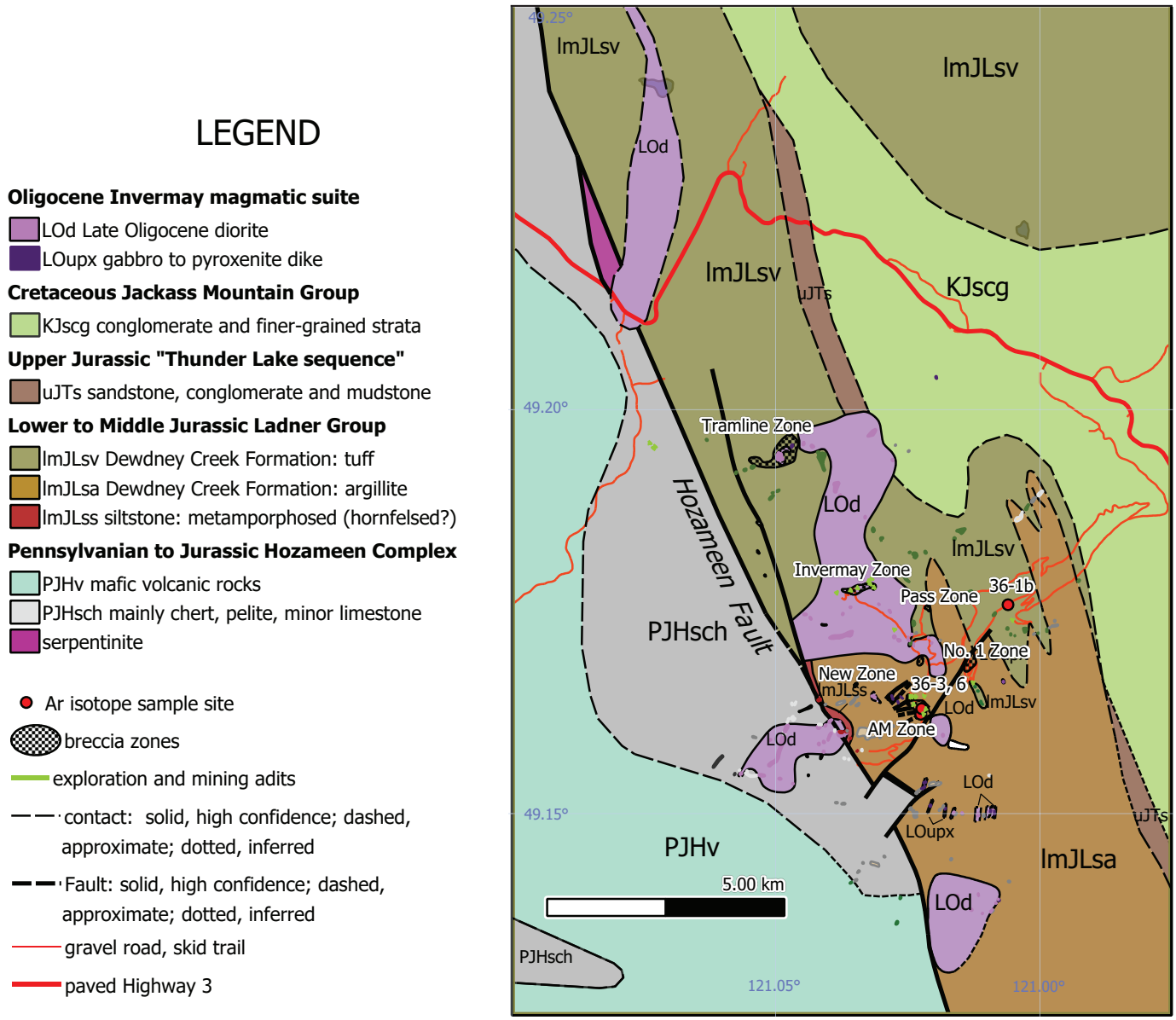

Fig. 3. Geologic setting of breccia zones at Giant Copper principally based on the distribution of rock units exposed in outcrops shown on property maps (and shown here) by Imperial Metals Corporation (e.g., Miller-Tait, 2016). Correlation with regional geological units is constrained by regional mapping by Cairnes (1924, 1944), Monger et al. (1989), and local property-scale observations.

In the Giant Copper area, both Hozameen and Methow terranes are intruded by the Invermay suite of plutons that have irregular outlines and are up to about 3 km long. If the main Hozameen fault trace has been mapped correctly, Invermay intrusions cut across the fault (Fig. 3).

3. $^{40}Ar/^{39}Ar$ analysis

3.1. $^{40}Ar/^{39}Ar$ analytical methods

Clean and fresh samples for $^{40}Ar/^{39}Ar$ analysis were crushed and sieved to 0.2-0.4 mm size fraction. Mineral separates were hand-picked, washed in acetone, dried, wrapped in aluminum foil and stacked in an irradiation capsule with similar-aged samples and neutron flux monitors (Fish Canyon Tuff sanidine; 28.02 Ma, (Renne et al., 1998).

The samples were irradiated in March 2007 at the McMaster Nuclear Reactor in Hamilton, Ontario, for 90 MWH, with a neutron flux of approximately $3x10^{16}$ neutrons/cm^2. Analyses (n=60) of 20 neutron flux monitor positions produced errors of <0.5% in the J value.

The samples were analyzed at the Noble Gas Laboratory, Pacific Centre for Isotopic and Geochemical Research, The University of British Columbia, Vancouver, BC, Canada. The mineral separates were step-heated at incrementally higher powers in the defocused beam of a 10W CO_2 laser (New Wave Research

MIR10) until fused. The gas evolved from each step was analyzed by a VG5400 mass spectrometer equipped with an ion-counting electron multiplier. All measurements were corrected for total system blank, mass spectrometer sensitivity, mass discrimination, radioactive decay during and subsequent to irradiation, as well as interfering Ar from atmospheric contamination and the irradiation of Ca, Cl and K (Isotope production ratios: $(^{40}Ar/^{39}Ar)_K$=0.0302 ±0.00006, $(^{37}Ar/^{39}Ar)_{Ca}$=1416.4 ±0.5, $(^{36}Ar/^{39}Ar)_{Ca}$=0.3952 ±0.0004, Ca/K=1.83 ±0.01 ($^{37}Ar_{Ca}/^{39}Ar_K$)).

Ages of heating steps were calculated using ArArCalc (Koppers, 2002). Release spectrum plateaus and correlation ages were calculated using Isoplot ver. 3.09 (Ludwig, 2003). Errors are quoted at the 2σ (95% confidence) level and are propagated from all sources except mass spectrometer sensitivity and age of the flux monitor. The most justifiable plateau and plateau age were picked based on the following criteria: three of more contiguous steps comprising more than 50% of the ^{39}Ar; the probability of fit of the weighted mean age greater than 5%; the slope of the error-weighted line through the plateau ages equals zero at 5% confidence; the ages of the two outermost steps on a plateau are not significantly different from the weighted-mean plateau age (at 1.8σ, six or more steps only); and the outermost two steps on either side of a plateau must not have nonzero slopes with the same sign (at 1.8σ, nine or more steps only).

3.2. $^{40}Ar/^{39}Ar$ geochronologic results

Complete details of the analyses, including inverse correlation plots, are presented in Gabites and Mihalynuk (2026). Plateau and correlation ages were calculated using Isoplot ver. 3.09 (Ludwig, 2003). Errors are quoted at the 2-sigma (95% confidence) level and are propagated from all sources except mass spectrometer sensitivity and age of the flux monitor.

3.2.1. Sample MMI06-36-1b Location, -121.00600°E, 49.17585°N; UTM zone 10, NAD 83: 645412 mE, 5448708 mN

Sample MMI06-36-1b is representative of the Invermay suite of hornblende and biotite porphyry intrusions. A biotite porphyritic intrusive sample was collected from the 1500-level dump for analysis. It is quartz->plagioclase->orthoclase->biotite-porphyritic and contains 1-2% chalcopyrite in tourmaline veinlets. Step heating results from sample MMI06-36-1b (Table 1; Fig. 4) give an age of 24.22 ±0.13 Ma from a 5-step plateau produced by 79.1% of the ^{39}Ar released.

3.2.2. Sample MMI06-36-3 Location, -121.02254°E, 49.16230°N; UTM zone 10, NAD 83: 644245 mE, 5447171 mN

Sample MMI06-36-3 is a rusty-weathering, dark grey-brown, medium-grained biotite hornfels (Fig. 5), part of the alteration assemblage related to intrusion and mineralization at the AM zone. Step heating results of biotite from sample MMI06-36-3 (Table 2; Fig. 6) indicate an undisturbed 6-step plateau

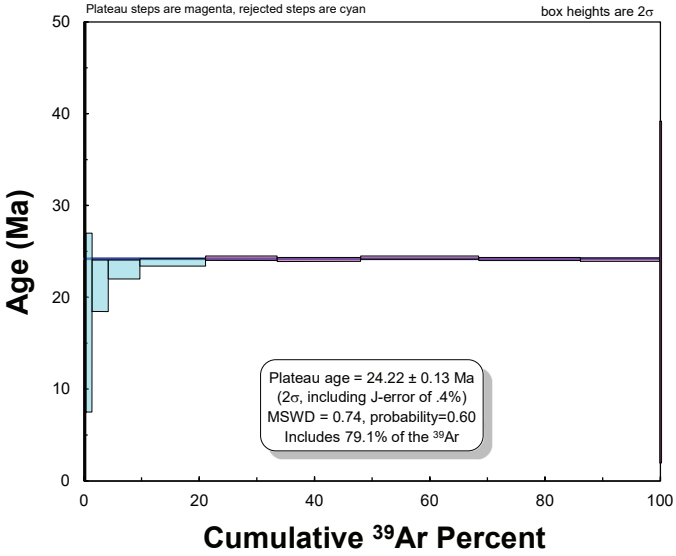

Fig. 4. Argon release spectrum from biotite phenocrysts of sample MMI06-36-1b. Low temperature steps trimmed to chart area. See Gabites and Mihalynuk (2026) for unmodified plot.

Fig. 5. Cut sample MMI06-36-3 biotite hornfels showing rusty weathering exterior and dark brown-grey interior. Biotite was extracted from this sample for $^{40}Ar/^{39}Ar$ analysis.

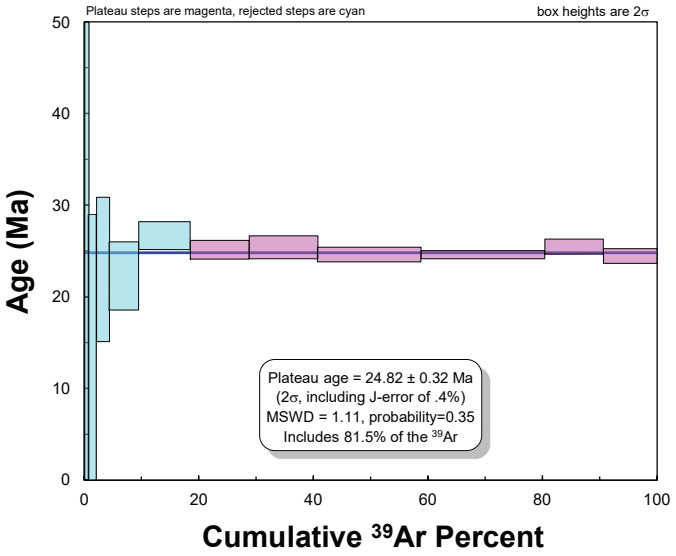

Fig. 6. Argon release spectrum from sample MMI06-36-1b. Low temperature steps trimmed to chart area. See Gabites and Mihalynuk (2026) for unmodified plot.

Table 1. $^{40}Ar/^{39}Ar$ analytical results from step heating of sample MMI06-36-1b. Analysis by Tom Ullrich, revised by Janet Gabites, Pacific Centre for Isotopic and Geochemical Research, The University of British Columbia.

MMI06-36-1b Biotite

Laser			Isotope Ratios												
Power(%)	40Ar/39Ar	2σ	36Ar/39Ar	2σ	39Ar/40Ar	2σ	36Ar/40Ar	2σ	Rho	K/Ca	%40Ar rad	f 39Ar	40Ar*/39ArK	Age	2σ
2.0	245.66	0.02	0.83100	0.04600	0.0041	0.0001	0.00338	0.00007	0.26	1.58	1.00	0.07	0.43	8.01	± 92.49
2.2	60.50	0.02	0.20500	0.09000	0.0168	0.0002	0.00336	0.00015	0.06	1.16	1.01	0.10	0.47	8.71	± 49.32
2.4	27.69	0.01	0.09100	0.04000	0.0363	0.0003	0.00327	0.00006	0.09	0.68	1.04	1.11	0.93	17.29	± 9.76
2.6	7.68	0.01	0.02200	0.04600	0.1318	0.0007	0.00288	0.00007	0.05	3.98	1.18	2.80	1.15	21.27	± 2.81
2.8	3.36	0.01	0.00700	0.05200	0.3031	0.0014	0.00212	0.00006	0.03	14.93	1.62	5.43	1.25	23.07	± 1.02
3.0	2.22	0.01	0.00300	0.04600	0.4592	0.0019	0.00141	0.00003	0.01	34.48	2.48	11.40	1.29	23.81	± 0.40
3.2	1.68	0.01	0.00100	0.06400	0.6108	0.0026	0.00071	0.00002	0.01	37.04	5.17	12.47	1.31	24.28	± 0.24
3.4	1.54	0.01	0.00100	0.08400	0.6697	0.0028	0.00047	0.00002	0.00	33.33	8.18	14.43	1.31	24.15	± 0.20
3.6	1.50	0.01	0.00100	0.09000	0.6847	0.0029	0.00038	0.00002	0.01	29.41	10.42	20.55	1.32	24.34	± 0.18
3.8	1.50	0.01	0.00100	0.08000	0.6837	0.0028	0.00040	0.00002	0.00	35.71	9.73	17.56	1.31	24.19	± 0.17
4.0	1.50	0.01	0.00100	0.09400	0.6867	0.0028	0.00039	0.00002	0.00	32.26	9.89	13.84	1.31	24.13	± 0.19
4.2	35.06	0.02	0.11500	0.06000	0.0290	0.0002	0.00328	0.00010	0.07	1.19	1.03	0.25	1.11	20.60	± 18.61

J = 0.010311 ± 0.000012; Volume 39ArK = 2583.76 x E-13 cm3 NPT

Integrated Date = 24.19 ± 0.08 Ma

Plateau age = 24.22 ± 0.13 Ma; (2σ, including J-error of .2%), MSWD = 0.74, probability = 0.60, Includes 79.1% of the 39Ar, steps 7 through 12

Inverse isochron (correlation age) results: Model 1 Solution (±95%-conf.) on 12 points

Age = 23.91 ± 0.10 Ma Initial 40Ar/36Ar = 290.8 ± 2.8; MSWD = 0.91, Probability = 0.52

Table 2. $^{40}Ar/^{39}Ar$ analytical results from step heating of sample MMI06-36-3. Analysis by Tom Ullrich, revised by Janet Gabites, Pacific Centre for Isotopic and Geochemical Research, The University of British Columbia.

MMI06-36-3 Biotite

Laser			Isotope Ratios												
Power(%)	40Ar/39Ar	2σ	36Ar/39Ar	2σ	39Ar/40Ar	2σ	36Ar/40Ar	2σ	Rho	K/Ca	%40Ar rad	f 39Ar	40Ar*/39ArK	Age	2σ
2.0	104.48	0.02	0.35400	0.04200	0.0095	0.0001	0.00338	0.00007	0.07	0.92	1.00	0.79	0.19	3.57	± 38.34
2.2	49.94	0.01	0.16800	0.04200	0.0201	0.0001	0.00335	0.00007	0.06	0.93	1.01	1.33	0.50	9.34	± 19.58
2.4	22.75	0.02	0.07300	0.04200	0.0444	0.0004	0.00320	0.00006	0.10	1.09	1.06	2.29	1.24	23.01	± 7.89
2.6	11.28	0.01	0.03400	0.04000	0.0898	0.0006	0.00303	0.00006	0.07	1.59	1.12	5.15	1.21	22.31	± 3.75
2.8	4.28	0.01	0.01000	0.05800	0.2393	0.0014	0.00224	0.00007	0.04	1.11	1.54	8.96	1.45	26.72	± 1.54
3.0	3.30	0.03	0.00700	0.05200	0.3116	0.0052	0.00199	0.00005	0.20	0.88	1.75	10.39	1.36	25.17	± 1.04
3.2	3.47	0.01	0.00700	0.06200	0.2949	0.0019	0.00205	0.00007	0.03	0.55	1.70	11.87	1.38	25.41	± 1.25
3.4	2.66	0.01	0.00500	0.05600	0.3851	0.0024	0.00173	0.00006	0.07	0.27	2.08	18.04	1.33	24.63	± 0.82
3.7	1.77	0.02	0.00200	0.09000	0.5850	0.0050	0.00081	0.00004	0.06	0.96	4.61	21.59	1.33	24.63	± 0.47
4.0	1.83	0.03	0.00200	0.14200	0.5736	0.0103	0.00077	0.00007	0.08	1.07	4.88	10.21	1.38	25.51	± 0.85
4.4	1.70	0.01	0.00100	0.20200	0.6251	0.0031	0.00064	0.00009	0.01	2.23	5.92	9.38	1.32	24.49	± 0.80

J = 0.010318 ± 0.00001; Volume 39ArK = 822.79 x E-13 cm3 NPT

Integrated Date = 24.87 ± 0.30 Ma

Plateau age = 24.82 ± 0.32 Ma; (2σ, including J-error of .2%), MSWD = 1.11, probability = 0.35, Includes 81.5% of the 39Ar, steps 6 through 11

Inverse isochron (correlation age) results: Model 1 Solution (±95%-conf.) on 11 points

Age = 24.30 ± 0.54 Ma Initial 40Ar/36Ar = 293.7 ± 4.4; MSWD = 1.9, Probability = 0.045

produced by 81.5% of the ^{39}Ar released. The plateau provides an age of 24.82 ±0.32 Ma. This age is very close to the age of the causative intrusion, (sample MMI06-36-1b), confirming the consanguinity interpreted from field relationships where the intrusion and coarse sulphides are intermingled (Fig. 7).

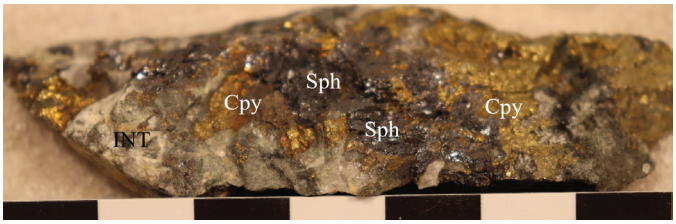

Fig. 7. Sample MMI06-36-2, showing coarse chalcopyrite (Cpy) and sphalerite (Sph) intergrown with Invermay intrusion (INT) shows consanguinity of mineralization and intrusion. Scale divisions are in cm.

3.2.3. Sample MMI06-36-6 Location, -121.02235°E, 49.16298°N; UTM zone 10, NAD 83: 644256 mE, 5447248 mN

This sample was obtained from diamond-drill hole DDH GCS06-02 at a recorded depth of 620 feet (189 m) in the AM zone. It is a sample of sedimentary host rock overprinted by pre- to syn-mineralization biotite hornfels. Textural relations show that biotite crystallization immediately preceded and accompanied mineralization and constrains the age of mineralization. Step heating results of biotite from sample MMI06-36-2 (Table 3; Fig. 8) show an 11-step plateau produced by 99.02% of the ^{39}Ar released. The plateau provides an age of 24.08 ±0.17 Ma. This age overlaps within errors the age of the Invermay suite intrusion, (sample MMI06-36-1b), again confirming the consanguinity interpreted from field relationships.

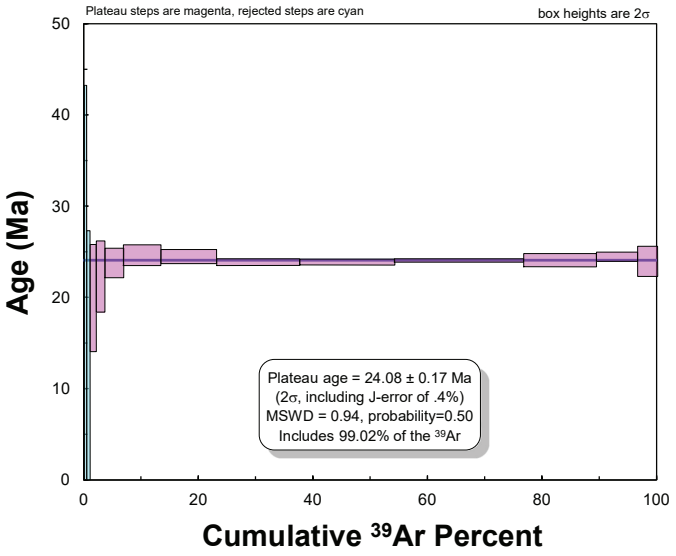

Fig. 8. Argon release spectrum from sample MMI06-36-6. Low temperature steps trimmed to chart area. See Gabites and Mihalynuk (2026) for unmodified plot.

Table 3. ^{40}Ar/^{39}Ar analytical results from step heating of sample MMI06-36-6. Analysis by Tom Ullrich, revised by Janet Gabites, Pacific Centre for Isotopic and Geochemical Research, The University of British Columbia.

MMI06-36-6 Biotite

Laser	*Isotope Ratios*														
Power(%)	*40Ar/39Ar*	*2 σ*	*36Ar/39Ar*	*2 σ*	*39Ar/40Ar*	*2 σ*	*36Ar/40Ar*	*2 σ*	*Rho*	*K/Ca*	*%40Ar rad*	*f 39Ar*	*40Ar*/39ArK*	*Age*	*2σ*
2.0	77.43	0.01	0.26400	0.04000	0.0131	0.0001	0.00339	0.00007	0.13	0.41	1.00	0.39	-0.19	-3.53	± 27.72
2.2	33.59	0.01	0.11200	0.04600	0.0305	0.0002	0.00331	0.00008	0.03	0.25	1.02	0.59	0.73	13.60	± 13.73
2.4	12.76	0.01	0.04100	0.05200	0.0817	0.0006	0.00309	0.00009	0.11	0.22	1.10	1.07	1.08	19.95	± 5.86
2.6	6.28	0.02	0.01800	0.08000	0.1698	0.0014	0.00271	0.00012	0.06	0.43	1.26	1.56	1.21	22.32	± 3.89
2.8	3.97	0.03	0.00900	0.06000	0.2657	0.0035	0.00225	0.00007	0.20	0.94	1.53	3.23	1.29	23.81	± 1.61
3.0	2.58	0.02	0.00400	0.08800	0.4069	0.0048	0.00159	0.00008	0.10	0.94	2.21	6.60	1.33	24.65	± 1.13
3.2	2.27	0.02	0.00400	0.07600	0.4593	0.0042	0.00138	0.00006	0.09	0.48	2.59	9.61	1.33	24.49	± 0.78
3.4	1.90	0.02	0.00200	0.04800	0.5481	0.0044	0.00105	0.00003	0.10	0.50	3.50	14.53	1.29	23.92	± 0.38
3.6	1.63	0.01	0.00100	0.06600	0.6408	0.0047	0.00065	0.00003	0.07	0.78	5.96	16.55	1.29	23.91	± 0.31
3.8	1.48	0.01	0.00100	0.08200	0.7023	0.0041	0.00036	0.00002	0.03	2.44	12.09	22.52	1.30	24.10	± 0.21
4.0	1.47	0.05	0.00100	0.24600	0.7203	0.0171	0.00027	0.00005	0.10	3.58	17.04	12.67	1.31	24.12	± 0.73
4.2	1.52	0.02	0.00100	0.21600	0.7108	0.0068	0.00027	0.00006	0.01	2.78	17.33	7.20	1.32	24.47	± 0.51
4.7	1.72	0.01	0.18000	0.36000	0.6578	0.0455	0.00056	0.00020	0.00	1.18	6.97	3.48	1.30	23.99	± 1.65

J = 0.010315±0.000012; Volume 39ArK = 1453.83 x E-13 cm3 NPT

Integrated Date = 24.08 ± 0.14 Ma

Plateau age = 24.08 ± 0.17 Ma; (2σ, including J-error of .2%), MSWD = 0.94, probability = 0.50, Includes 99.02% of the 39Ar, steps 3 through 13

Inverse isochron (correlation age) results: Model 1 Solution (±95%-conf.) on 13 points

Age = 23.59 ± 0.16 Ma Initial 40Ar/36Ar = 290.6 ± 14; MSWD = 0.91, Probability = 0.53

4. Discussion

4.1. Breccia pipe relation to porphyry copper systems

Porphyry deposits typically form within a subduction-related volcanic arc, or continentward of the arc, where they are attributed to a shallowly dipping or flat subducted slab segment, but uncertainties persist in flat-slab models that project porphyry deposit formation far inland of the active margin (e.g., Glazner, 2022). Classical calc-alkalic porphyry deposits formed in a normal volcanic arc setting are enriched in one or more of copper, molybdenum, gold, and silver. Other base metals (e.g., lead and zinc) may occur in these porphyry deposits, mainly as sulphides, but they rarely constitute a substantial byproduct, except where distal veins and replacement zones are well-developed (e.g., Bisbee and Cochise, Warren district, Stegen et al., 2005); typical of carbonate replacement-style mineralization in mantos and chimneys distal to copper porphyry deposits (Lefebure and Jones, 2020). More evolved granitoids, especially those having a continental crustal component and historically attributed to flat-slab subduction, may comprise tin, tungsten, and molybdenum porphyry deposits, in which silver, copper, lead, and zinc sulphides can be important ore constituents (e.g., Climax, Colorado, White et al., 1981; Potosi, Bolivia, Lehman, 1994; Mount Pleasant, New Brunswick, Sinclair, 1994). Polymetallic porphyry-related tourmaline breccia pipe deposits are intermediate in ore metal diversity and tectonic setting between these two major classes of porphyry deposits and share common characteristics (Sillitoe and Sawkins, 1974; Sillitoe, 1985). These breccia pipe deposits can have distinctive geochemical footprints and occur within well-defined belts superimposed on older arc strata, such as in the ancestral Cascades of southern British Columbia and Washington state (Fig. 9) and other arcs globally.

4.2. Syn-kinematic intrusion and faulting

The age data presented here are consistent with the LA-ICP-MS U-Pb age from the Invermay intrusive suite presented by Fischer (2022), ending speculation that mineralization is related to Late Cretaceous intrusions (e.g., Robertson, 2006), which was based on a K-Ar biotite age of 85.7 ±6 Ma by Wanless et al. (1967) from a body 6 km to the northwest.

Regionally, the small Invermay suite intrusive bodies in the Giant Copper area are dwarfed by the well-known, coeval Chilliwack batholith extending across the international border 15 to 45 km to the southwest, and apparently stitching together Hozameen (Bridge River), Shuksan, and Chilliwack terranes (Fig. 1) by Oligocene. Co-magmatic volcanic rocks (22-21 Ma) are felsic to intermediate pyroclastics and flows of the Coquihalla Formation. To the north, these rocks rest atop Methow terrane and the Eagle Plutonic complex (Monger, 1989). To the south in Washington state, Haugerud and Tabor, 2009, mapped the equivalent Ohanapecosh volcanic rocks east of the Hozameen terrane, where they rest on Methow terrane. The southern extents of the Hozameen terrane are mapped as a thrust sheet underlain by Methow basin and metamorphosed equivalents (Fig. 2). Where metamorphosed Methow extends beneath and west of the Hozameen thrust sheet, it is extensively overlain by Ohanapecosh volcanic strata and is also cut by co-magmatic Snoqualmie intrusions. At Giant Copper, the Invermay intrusions cut the western terrane-bounding Hozameen fault but are also cut by a splay of the fault that extends into the Methow terrane (Fig. 3). Thus, a late syn-kinematic relationship between intrusion and faulting is suggested.

4.3. Oligocene magmatism and mineralization in the Cordillera

Oligocene porphyry deposits are not well known in the Canadian Cordillera. In British Columbia, they are overshadowed by the prolific Late Triassic-Early Jurassic porphyry epoch (Logan and Mihalynuk, 2014). However, in the US Cordillera, Bingham (Utah), the world's seventh largest copper deposit (Cooke et al., 2005; second in terms of contained gold), is also Oligocene to Late Eocene, with mineralization dated at 37.0 ±0.27 Ma, and the host intrusions having formed in less than a third of a million years, between 38.10 and 37.78 Ma (von Quadt et al., 2011). Closer to Giant Copper, Oligocene Coquihalla volcanic units and co-magmatic Chilliwack intrusions are part of the ancestral Cascade arc, best known in the Pacific northwest USA (Fig. 9). The arc has traditionally been divided into the Eocene to Miocene western Cascades or 'Ancestral Cascades arc' (Stern and Dumitru, 2019) , and the Pliocene to Holocene High Cascades (Tepper and Clark, 2024).

In Washington state, rocks coeval with the Invermay suite include the 'Snoqualmie family' of intrusive rocks (Oligocene-Miocene; Haugerud and Tabor, 2009) which cut Hozameen Group rocks. Coeval volcanic strata of the 'Ohanapecosh episode' (Oligocene) are considered the oldest volcanic rocks of the Cascade magmatic arc and may have been cannibalized by co-magmatic Snoqualmie intrusions (28-22 Ma, Haugerud and Tabor, 2009). The oldest part of the ancestral Cascade arc are 35-29 Ma plutons of the "Index family" (Haugerud and Tabor, 2009), but coeval volcanic rocks have apparently all been removed by erosion. Both Index and Snoqualmie intrusions are responsible for several other examples of mineralized tourmaline breccias as compiled by Singer et al. (2008) and Fischer (2022) from Black Jack (19.6 Ma, near Portland, 45.5°N) to Sunrise (28.2 Ma, 48.2°N), and porphyry copper deposits, from Margaret (21 Ma, 46.4°N) to North Fork (25 Ma, 47.7°N), and Glacier Peak (23.3 Ma, 48.2°N).

Attempts to address the plate tectonic setting of the ancestral Cascades commonly do not consider the old arc units as extending into northernmost Washington State and southern British Columbia (e.g., Madsen et al., 2006; Stern and Dumitru, 2019; Humphreys and Grunder, 2022). In contrast, regional mapping and isotopic age compilations by Haugerud and Tabor (2009) and Monger (1989) show Oligocene extrusive and intrusive rocks that are a northern extension of the ancestral Cascade belt. In particular, intrusive rocks thought to be the comagmatic with Coquihalla Formation extend as far north as Hells Gate on the Fraser River (~10 km south of Boston Bar, Fig. 9).

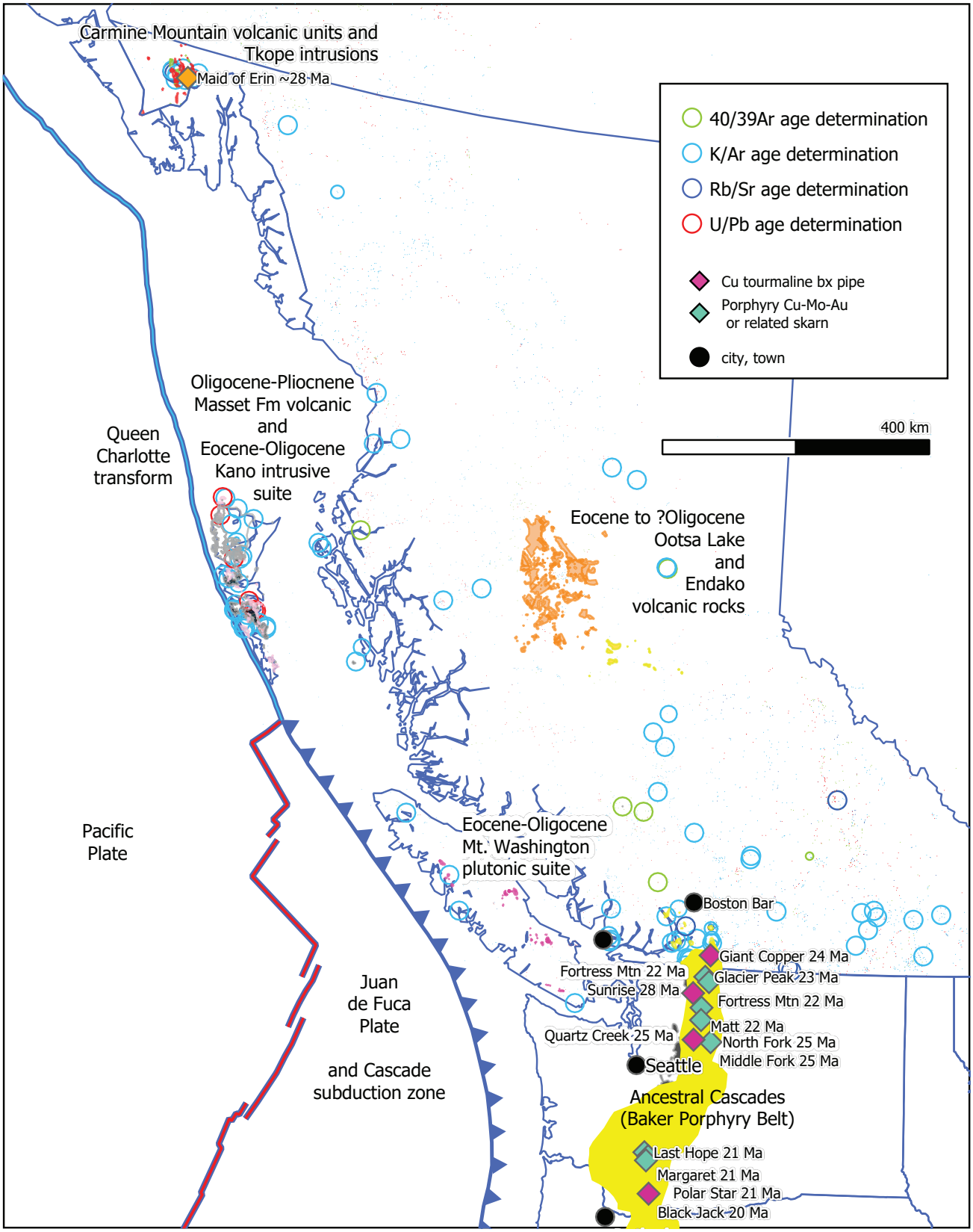

Fig. 9. Distribution of the ancestral Cascade belt magmatic rocks in British Columbia, Washington State, and Oregon (45-5 Ma volcanic and intrusive rocks combined, after Stern and Dumitru, 2019); age data from Engels et al. (1976), Mullen et al. (2018). Distribution of Oligocene ages in British Columbia are from Han et al. (2020). Copper porphyry and breccia deposits in Washington and Oregon from Singer et al. (2008), Lasmanis (1995), and Iveson et al. (2016).

What the true northern extent of the ancestral Cascade arc in British Columbia actually is, and what the plate tectonic explanation for the paleogeographic limit of Cascade subduction is, are unanswered questions and beyond the scope of this paper. However, Oligocene magmatism and mineralization span the length of western British Columbia (Fig. 9), and at several localities Oligocene intrusions are related to mineralization with past production.

4.3.1. Tkope suite and Carmine Mountain volcanic feeders

In the far northwest part of the province, Tkope suite tonalite and quartz monzonite intrusions are associated with skarn mineralization; some zones have small tonnage past production (Fig. 9). Examples include the Maid of Erin (or Carmichael, Rainy Hollow) and State of Montana (or Arizona, Montana, Rainy Hollow). Sulphide minerals in garnet-epidote skarn are bornite, chalcopyrite, sphalerite, and in some instances, argentiferous wittichenite (Cu_3BiS_3) and gold (cf. MINFILE 114P 007 and 008). Breccia is noted at the Maid of Erin (Wilson, 1983, Figure 015-83-17) and, at the Bornite prospect (or Cat, Horrible; MINFILE 114P 019), extensive intrusive breccias and skarn contain copper, molybdenum, lead, zinc, silver, and gold mineralization interpreted as related to a porphyry system.

Co-magmatic volcanic rocks found in the same region are named after a prominent massif, Carmine Mountain. Porphyry dikes, feeders to the volcanic rocks that underlie Carmine Mountain, are associated with silver- and gold-enriched epidote-diopside skarn containing pods of galena, sphalerite and chalcopyrite (Fair prospect, MINFILE 114P 070), but with no record of past production.

4.3.2. Nechako suite

Perhaps the most extensive Oligocene rocks are those of the Nechako suite in central British Columbia. However, most related mineralization is precious metal, low sulphidation epithermal in nature. Porphyry copper prospects in the area have no clear association with this Oligocene suite.

5. Summary

Geochronological data presented here confirm the Oligocene age of the Invermay intrusive suite at the past-producing Giant Copper deposit and show that the breccia pipe mineralization has the same age. The Invermay suite is part of ancestral Cascade arc volcanic rocks, intrusions, and related breccia and porphyry mineralization that extend into Washington and Oregon. The northern limits of the ancestral Cascade arc probably stretch at least to Hell's Gate (49.8°N). Oligocene magmatic rocks are known to extend the length of western British Columbia, and Oligocene intrusive-related polymetallic deposits with past production are known from both ends of the province.

Acknowledgments

The lead author thanks Imperial Metals Corporation for the invitation to visit the Giant Copper deposit and the willingness of their geological team to share technical information. The field program was facilitated by David Lefebure who also contributed to field discussions and aided in the collection of samples at Giant Copper. Tom Ullrich conducted the $^{40}Ar/^{39}Ar$ analysis of the samples reported here.

References cited

Cairnes, C.E., 1920. Coquihalla Area, British Columbia. In: Geological Survey of Canada, Summary Report, 1920, Part A, pp. 24-42.

Cairnes, C.E., 1924. Coquihalla Area, British Columbia. Geological Survey of Canada, Memoir 139, 187 p.

Cairnes, C.E., 1929. The Serpentine Belt of Coquihalla Region, Yale District, British Columbia. In: Geological Survey of Canada, Summary Report, Part A; pp. 144-197.

Cairnes, C.E., 1944. Hope, Yale and New Westminster Districts, British Columbia. Geological Survey of Canada, Map 737A.

Coates, J.A., 1974. Geology of the Manning Park area, British Columbia. Geological Survey of Canada, Bulletin 238, 177 p.

Cohen, K., Harper, D., Gibbard, P., and Car, N., 2025. The ICS international chronostratigraphic chart this decade. Episodes, 48, 105-114. <https://doi.org/10.18814/epiiugs/2025/025001>

Colpron, M., 2020. Yukon terranes-A digital atlas of terranes for the northern Cordillera. Yukon Geological Survey. <https://data.geology.gov.yk.ca/Compilation/2#InfoTab>

Cooke, D.R., Hollings, P., and Walshe, J.L., 2005. Giant porphyry deposits: Characteristics, distribution, and tectonic controls. Economic Geology, 100, 801-818.

Engels, J.C., Tabor, R.W., Miller, F.K., and Obradovich, J.D., 1976. Summary of K-Ar, Rb-Sr, U-Pb, and fission-track ages of rocks from Washington State prior to 1975 (exclusive of Columbia Plateau Basalts); U.S. Geological Survey Miscellaneous Field Studies Map MF-710, 1:500,000 scale.

Fischer, W.T., 2022. Tourmaline breccia pipes of the giant copper property, Southern British Columbia: Understanding the significance of tourmaline and breccia pipes as vectoring tools in porphyry copper deposits. Ph.D. thesis, Simon Fraser University, Burnaby, British Columbia, Canada, 318 p.

Fischer, W.T., Marshall, D.D., Hanchar, J.M., Riley, D. and Hiebert, S., 2023. Differentiating tourmaline species via chemistry and reflectance spectroscopy at the Giant Copper porphyry deposit and associated tourmaline breccia pipes: Testing tourmaline as a mineral vector. Economic Geology, 118, 883-902.

Fischer, W.T., Marshall, D.D., and Miller-Tait, J., 2024. Tourmaline breccia pipes of the Giant Copper porphyry system: Extending the Cascadia porphyry district into southern British Columbia, Canada. CIM Journal, 15, 136-157.

Frikken, P.H., Cooke, D.R., Walshe, J.L., Archibald, D., Skarmeta, J., Serrano, L., and Vargas, R., 2005. Mineralogical and isotopic zonation in the Sur-Sur tourmaline breccia, Río Blanco-Los Bronces Cu-Mo deposit, Chile: Implications for ore genesis. Economic Geology, 100, 935-961.

Gabites, J.E., and Mihalynuk, M.G., 2026. $^{40}Ar/^{39}Ar$ geochronologic data from samples collected at Giant Copper. British Columbia Ministry of Mining and Critical Minerals, British Columbia Geological Survey GeoFile 2026-in press.

Glazner, A.F., 2022, Cenozoic magmatism and plate tectonics in western North America: Have we got it wrong? In: Foulger, G.R., Hamilton, L.C., Jurdy, D.M., Stein, C.A., Howard, K.A., and Stein, S., (Eds.), In the Footsteps of Warren B. Hamilton: New Ideas in Earth Science. Geological Society of America Special

Paper 553, pp. 1-14. <https://doi.org/10.1130/2021.2553(09)>
Greig, C.J., Armstrong, R.L., Harakal, J.E., Runkle, D., and der Heyden, P.V., 1992. Geochronometry of the Eagle plutonic complex and the Coquihalla area, southwestern British Columbia. Canadian Journal of Earth Sciences, 29, 812-829.
Han, T., Ootes, L., and Yun, K., 2020. The British Columbia Geological Survey geochronologic database: Preliminary release of ages. British Columbia Ministry of Energy, Mines and Low Carbon Innovation, British Columbia Geological Survey GeoFile 2020-10, 4 p.
Haugerud, R.A., and Tabor, R.W., 2009. Geologic map of the north Cascade Range, Washington. US Department of the Interior, US Geological Survey, Scientific Investigations, Map 2940, 29 p.
Humphreys, E.D., and Grunder, A.L., 2022. Tectonic controls on the origin and segmentation of the Cascade Arc, USA. Bulletin of Volcanology, 84, 102. <https://doi.org/10.1007/s00445-022-01611-2>
Hurlow, H.A., and Nelson, B.K., 1993. U-Pb zircon and monazite ages for the Okanogan Range batholith, Washington: Implications for the magmatic and tectonic evolution of the southern Canadian and northern United States Cordillera. Geological Society of America Bulletin, 105, 231-240.
Imperial Metals Corporation, 2022. News Release: 2022.01.19 Imperial to Surrender Giant Copper Property. <https://imperialmetals.com/assets/docs/2022.01.19%20Imperial%20to%20Surrender%20Giant%20Copper%20Property.pdf>
Iveson, A.A., Webster, J.D., Rowe, M.C., and Neill, O.K., 2016. Magmatic-hydrothermal fluids and volatile metals in the Spirit Lake pluton and Margaret Cu-Mo porphyry system, SW Washington, USA. Contributions to Mineralogy and Petrology, 171, 20 p. <https://doi.org/10.1007/s00410-015-1224-6>
Koppers, A.A.P., 2002, ArArCALC-software for $^{40}Ar/^{39}Ar$ age calculations. Computers and Geosciences, 28, 605-619.
Lasmanis, R., 1995. Regional geological and tectonic setting of porphyry deposits in Washington State. In: Schroeter, T.G., (Ed.), Porphyry deposits of the northwestern Cordillera of North America: Canadian Institute of Mining, Metallurgy and Petroleum Special Volume, 46, pp. 77-102.
Lefebure, D.V., and Jones, L.D., (compilers), 2022. British Columbia Geological Survey mineral deposit profiles, 1995 to 2012; updated with new profiles for VMS, porphyry, and mafic-ultramafic deposits. British Columbia Ministry of Energy, Mines and Low Carbon Innovation, British Columbia Geological Survey GeoFile 2020-11, 652 p.
Lehmann, B., 1994. Petrochemical factors governing the metallogeny of the Bolivian tin belt. In: Reutter, K-J., Scheuber, E., and Wigger, P.J., (Eds.), Tectonics of the Southern Central Andes. Structure and Evolution of an Active Continental Margin. Springer-Verlag, Berlin and Heidelberg, pp. 317-326.
Logan, J.M., and Mihalynuk, M.G., 2014. Tectonic controls on early Mesozoic paired alkaline porphyry deposit belts (Cu-Au ±Ag-Pt-Pd-Mo) within the Canadian Cordillera. Economic Geology, 109, 827-858.
Ludwig, K.R., 2003. Isoplot 3.09 A Geochronological Toolkit for Microsoft Excel. Berkeley Geochronology Center, Special Publication No. 4.
Madsen, J.K., Thorkelson, D.J., Friedman, R.M., and Marshall, D.D., 2006. Cenozoic to Recent plate configurations in the Pacific Basin: Ridge subduction and slab window magmatism in western North America. Geosphere, 2, 11-34.
Miller-Tait, J., 2016, Geochemical Assessment Report (2015 Soil Sampling Program) on the Giant Copper Property. British Columbia Ministry of Mining and Critical Minerals, Assessment Report 36083, 74 p.
MINFILE. Mineral Inventory. British Columbia Ministry of Mining and Critical Minerals, British Columbia Geological Survey. <https://www2.gov.bc.ca/gov/content/industry/mineral-exploration-mining/british-columbia-geological-survey/mineralinventory> (last accessed July 2025).
Monger, J.W.H., and Brown, W.H., 2016. Tectonic Evolution of the Southern Coast-Cascade Orogen, Northwestern Washington and Southwestern British Columbia. The Geology of Washington and Beyond: From Laurentia to Cascadia, University of Washington Press, Volume 10, pp. 101-130.
Monger, J.W.H., 1989. Hope map area. Geological Survey of Canada, Open File Map 41-1989, 1:250,000 scale.
Mullen, E.K., Paquette, J.L., Tepper, J.H., and McCallum, I.S., 2018. Temporal and spatial evolution of Northern Cascade Arc magmatism revealed by LA-ICP-MS U-Pb zircon dating. Canadian Journal of Earth Sciences, 55, 443-462.
O'Brien, J.A., 1987. Jurassic biostratigraphy and evolution of the Methow Trough, southwestern British Columbia. M.Sc. thesis, The University of Arizona, Tucson, 170 p.
O'Brien, J.A., Gehrels, G.E., and Monger, J.W.H., 1992. U-Pb geochronology of plutonic clasts from conglomerates in the Ladner and Jackass Mountain groups and the Peninsula Formation, southwestern British Columbia. In: Current Research, Part A, Geological Survey of Canada Paper 92-1A, pp. 209-214.
Oliver, S.L., 2011. The Eastgate-Whipsaw metamorphic belt as Paleozoic underpinnings to the Nicola Group. M.Sc. thesis, The University of British Columbia, Vancouver, 109 p.
Pinsent, R.H., 1998. Exploration and development highlights southwestern British Columbia, 1997. In: Exploration in British Columbia 1997, British Columbia Ministry of Energy and Mines, British Columbia Geological Survey, pp. 53-64.
Ray, G.E., 1986. The Hozameen fault system and related Coquihalla serpentine belt of southwestern British Columbia. Canadian Journal of Earth Science, 23, 1022-1041.
Ray, G.E., 1990. The geology and mineralization of the Coquihalla gold belt and Hozameen fault system, southwestern British Columbia. British Columbia Ministry of Energy, Mines and Petroleum Resources, British Columbia Geological Survey Bulletin 79, 109 p.
Renne, P.R., Swisher, C.C., III, Deino, A.L., Karner, D.B., Owens, T., and DePaolo, D.J., 1998. Intercalibration of standards, absolute ages and uncertainties in $^{40}Ar/^{39}Ar$ dating. Chemical Geology, 145, 117-152.
Robertson, S., 2006. Giant Copper Property, Southern British Columbia: Imperial Metals Corporation, 43-101 Technical Report, 47 p.
Schmitt, H.R., and Koyanagi, V.M., 1992. Cascade Recreation Area, preliminary geology and mineral potential. In: Geological Fieldwork 1991. British Columbia Ministry of Energy, Mines and Petroleum Resources, British Columbia Geological Survey Paper 1992-01, pp. 47-64.
Sillitoe, R.H., and Sawkins, F.J., 1974. Geologic, mineralogic, and fluid inclusion studies relating to the origin of copper-bearing tourmaline breccia pipes, Chile. Economic Geology, 66, 1028-1041.
Sillitoe, R.H., 1985. Ore-related breccias in volcanoplutonic arcs. Economic Geology, 80, 1467-1514.
Sinclair, W.D., 1994. Tungsten-molybdenum and tin deposits at Mount Pleasant, New Brunswick, Canada: Products of ore-fluid evolution in a highly fractionated granitic system. In: Seltmann, Käampf, and Möller, (Eds.), Metallogeny of Collisional Orogens, Czech Geological Survey, Prague, pp. 410-417.
Singer, D.A., Berger, V.I., and Moring, B.C., 2008. Porphyry copper deposits of the world: Database and grade and tonnage models, 2008. US Geological Survey Open File Report 2008-1155, 45 p., and digital files.

Stegen, R.J., Wright, E., and Bryant, D.G., 2005. Field guide to the Warren (Bisbee) Mining District, Cochise County, Arizona. Guidebook for the Arizona Geological Society, Spring Field Trip, April 30, 2005, 41 p.

Stern, R.J., and Dumitru, T.A., 2019. Eocene initiation of the Cascadia subduction zone: A second example of plume-induced subduction initiation? Geosphere, 15, 659-681.

Surpless, K.D., Sickmann, Z.T., and Koplitz, T.A., 2014. East-derived strata in the Methow basin record rapid mid-Cretaceous uplift of the southern Coast Mountains batholith. Canadian Journal of Earth Science, 51, 339-357.

Tabor, R.W., and Haugerud, R.A., 2016. Geology of the North Cascades-summary and enigmas. In: Cheney, E., (Ed.), Geology of Washington, University of Washington Press, Seattle, pp. 131-155.

Tabor, R.W., Haugerud, R.A., Hildreth, W., and Brown, E.H., 2003. Geologic Map of the Mount Baker 30′ × 60′ Quadrangle, Washington. U.S. Geological Survey Geologic Investigations Series I-2660, 1:100,000 scale, 2 sheets, 73 p.

Tepper, J.H., and Clark, K.P., 2024. Initiation of the Cascade arc. Geology, 52, 297-301. <https://doi.org/10.1130/G51888.1>

Umhoefer, P.J., and Miller, R.B., 1996. Mid-Cretaceous thrusting in the southern Coast Belt, British Columbia and Washington, after strike-slip fault reconstruction. Tectonics, 15, 545-565.

Umhoefer, P.J., and Schiarizza, P., 1996. Latest Cretaceous to early Tertiary dextral strike-slip faulting on the southeastern Yalakom fault system, southeastern Coast Belt, British Columbia. Geological Society of America Bulletin, 108, 768-785.

von Quadt, A., Erni, M., Martinek, K., Moll, M., Peytcheva, I., and Heinrich, C.A., 2011. Zircon crystallization and the lifetimes of ore-forming magmatic-hydrothermal systems. Geology, 39, 731-734.

Wanless, R.K., Stevens, R.D., Lachance, G.R., and Edmonds, C.M., 1967. Age determinations and geological studies K-Ar Isotopic ages, Report 7. Geological Survey of Canada, Paper, 66-17, 120 p. <https://doi.org/10.4095/100968>

Wheeler, J.O., Brookfield, A.J., Gabrielse, H., Monger, J.W.H., Tipper, H.W., and Woodsworth, G.J., 1991. Terrane map of the Canadian Cordillera, Geological Survey of Canada, “A” Series Map 1713A, 1:2,000,000 scale, 2 sheets.

White, W.H., Bookstrom, A.A., Kamilli, R.J., Ganster, M.W., Smith, R.P., Ranta, D.E., and Steininger, R.C., 1981. Character and origin of Climax-type molybdenum deposits. Economic Geology, 75th anniversary volume, 270-316.

Wilson, J.R., 1983. Diamond Drilling Assessment Report on (a) ME 2 Group Mineral Claims (b) ME 7 Group Mineral Claims. British Columbia Ministry of Mining and Critical Minerals, British Columbia Geological Survey, Assessment Report 11835, 15 p.

Zagorevski, A., van Staal, C.R., Bédard, J.H., Bogatu, A., Canil, D., Coleman, M., Golding, M., Joyce, N.L., Lawley, C., McGoldrick, S., Mihalynuk, M.G., Milidragovic, D., Parsons, A., and Schiarizza, P., 2021. Overview of Cordilleran oceanic terranes and their significance for the tectonic evolution of the northern Cordillera. In: Ryan, J.J., and Zagorevski, A., (Eds.), Northern Cordillera geology: A Synthesis of Research from the Geo-mapping for Energy and Minerals program, British Columbia and Yukon. Geological Survey of Canada, Bulletin 610, pp. 21-65.